

# Abyssal Stratification Change in the Southwest Pacific Basin

Helen Jingyi Zhang<sup>1</sup>, Caitlin Whalen<sup>2</sup>, Nirnimesh Kumar<sup>2</sup>, and Sarah G. Purkey<sup>3</sup>

<sup>1</sup>University of Washington Applied Physics Laboratory

<sup>2</sup>University of Washington

<sup>3</sup>Scripps Institution of Oceanography, UCSD

November 22, 2022

## Abstract

As abyssal ocean properties are altered by climate change, density stratification may be expected to change in response. This shift can affect the buoyancy flux, internal wave generation, and turbulent dissipation, which may impact mixing and vertical transport. In this study, repeated surveys of three hydrographic sections in the Southwest Pacific Basin between the 1990s-2010s are used to estimate the change in buoyancy frequency  $N$ . We find that below  $\Theta = 0.8^\circ\text{C}$ ,  $N$  is reduced by a mean scaling factor of  $0.88 \pm 0.06$  per decade. This reduction is intensified at depth, with the biggest change observed at  $\Theta = 0.63^\circ\text{C}$  by a scaling factor of  $0.71 \pm 0.07$ . Within the same time period, the magnitude of per unit area vertical diffusive heat flux is reduced by about  $0.01 \text{ Wm}$ , although this estimate is sensitive to the choice of estimated diffusivity. Finally, implications on heat budget and global ocean circulation are qualitatively discussed.

# 1 Abyssal Stratification Change in the Southwest Pacific 2 Basin

3 Helen. J. Zhang<sup>1</sup>, Caitlin. B. Whalen<sup>1</sup>, Nirnimesh Kumar<sup>2</sup>, Sarah. G.  
4 Purkey<sup>3</sup>

5 <sup>1</sup>Applied Physics Laboratory, University of Washington

6 <sup>2</sup>Civil and Environmental Engineering, University of Washington

7 <sup>3</sup>Scripps Institution of Oceanography, University of California, San Diego

## 8 **Key Points:**

- 9 • A decadal stratification decrease estimated from 25 years of repeat hydrography  
10 is observed in the abyssal Southwest Pacific Basin
- 11 • This change is significant below  $\Theta = 0.75$  °C and intensifies with depth to a per  
12 decade scaling factor of  $0.71 \pm 0.07$  by  $\Theta = 0.65$  °C
- 13 • Vertical diffusive heat flux is also reduced during the same time period by about  
14  $0.01 \text{ Wm}^{-2}/\text{decade}$

---

Corresponding author: H.J Zhang, [hjzhang@uw.edu](mailto:hjzhang@uw.edu)

**Abstract**

As abyssal ocean properties are altered by climate change, density stratification may be expected to change in response. This shift can affect the buoyancy flux, internal wave generation, and turbulent dissipation, which may impact mixing and vertical transport. In this study, repeated surveys of three hydrographic sections in the Southwest Pacific Basin between the 1990s-2010s are used to estimate the change in buoyancy frequency  $N^2$ . We find that below  $\Theta = 0.8$  °C,  $N^2$  is reduced by a mean scaling factor of  $0.88 \pm 0.06$  per decade. This reduction is intensified at depth, with the biggest change observed at  $\Theta = 0.63$  °C by a scaling factor of  $0.71 \pm 0.07$ . Within the same time period, the magnitude of per unit area vertical diffusive heat flux is reduced by about  $0.01 \text{ Wm}^{-2}$ , although this estimate is sensitive to the choice of estimated diffusivity. Finally, implications on heat budget and global ocean circulation are qualitatively discussed.

**Plain Language Summary**

Since the 1990s, the coldest water mass, which originates off Antarctica and fills most of the world's deepest ocean basins, has warmed significantly. Since cold water is denser and heavier, this observed warming has caused the deepest ocean water to lighten, altering the vertical structure of the water column. Using repeated ship-based measurements of temperature, salinity, and pressure, we find a weakening vertical density gradient in the very deep Southwest Pacific Basin between the 1990s-2010s. As a result, water near the seafloor became more homogeneous. This impacts the water's buoyancy and reduces the deep ocean's ability to mix in heat from above. Since large scale currents in the deep ocean are primarily driven by density differences and vertical mixing, the observed change may impact the global ocean circulation. This can have implications for deep ocean heat storage and future climate projections.

**1 Introduction**

Since the 1950s, more than 90% of the observed warming on Earth has occurred in the ocean, with one-third of the heat uptake going into waters below 4000 m (Purkey & Johnson, 2010; D. G. Desbruyères et al., 2016). Increased glacial melting has also produced a flux of freshwater off Antarctica and into the Southern Ocean (Jacobs & Giulivi, 2010; Purkey & Johnson, 2013; Rignot et al., 2019). This local warming and freshening

45 is transported globally via the Meridional Overturning Circulation (hereinafter MOC).  
46 The MOC is a balance between the renewal of cold water and diapycnal mixing of heat,  
47 therefore it is sensitive to changes in water temperature and salinity, which can affect  
48 its overall heat and volume transport (Munk, 1966; Lumpkin & Speer, 2007). Since the  
49 1990s, numerous studies have noted a contraction of abyssal northward flow, the bot-  
50 tom branch of the MOC (Johnson et al., 2008; Kouketsu et al., 2009; Purkey & John-  
51 son, 2012). Large scale shifts in temperature and salinity can change the structure of the  
52 water column by altering the vertical density gradient, or stratification. This has impli-  
53 cations for abyssal upwelling, which sets the strength of the MOC (Talley et al., 2003;  
54 Lumpkin & Speer, 2007). However, no observational studies to our knowledge have fo-  
55 cused on the role of changing climate on the strength of deep ocean stratification.

56 Past analysis of global temperature and salinity have shown that their changes are  
57 non-uniform throughout the water column, with a local maximum in warming and fresh-  
58 ening observed along the pathway of Antarctic Bottom Water (AABW) (Purkey & John-  
59 son, 2010; Kouketsu et al., 2011; Purkey & Johnson, 2013; D. Desbruyères et al., 2017).  
60 This dense water mass is formed from cold and saline water off Antarctica in the Ross  
61 Sea and along the Adelie Coast, sinking down the continental slope and flowing north-  
62 ward along deep western boundary currents (DWBC) (Orsi et al., 1999; Talley, 2013).  
63 As AABW travels north, diapycnal mixing brings in heat from above, lightening the bot-  
64 tom water and driving upwelling (Munk, 1966; Lumpkin & Speer, 2007). This process  
65 ventilates the abyssal ocean forming the upwards branch of the overturning circulation  
66 (Nikurashin & Ferrari, 2013; De Lavergne et al., 2016). As a consequence, this bottom  
67 water is newer than the deep waters above (England, 1995). Due to Antarctica’s accel-  
68 erated warming and freshening from melt-water, AABW production has slowed signif-  
69 icantly (Purkey & Johnson, 2012; Jacobs & Giulivi, 2010), although salinity in some source  
70 regions have rebounded in the last decade (Castagno et al., 2019). While the time scale  
71 of the MOC is multi-centennial, models have shown that the warm anomaly from changes  
72 in deep water production rate can propagate from the Adelie Coast to the North Pacific  
73 in as little as 40 years (Masuda et al., 2010). Therefore, recent climate changes near Antarc-  
74 tica can have a global effect on timescales within a few decades, and fingerprints of these  
75 changes can be observed in the time-span of global data collection (Johnson et al., 2007;  
76 Purkey & Johnson, 2010).

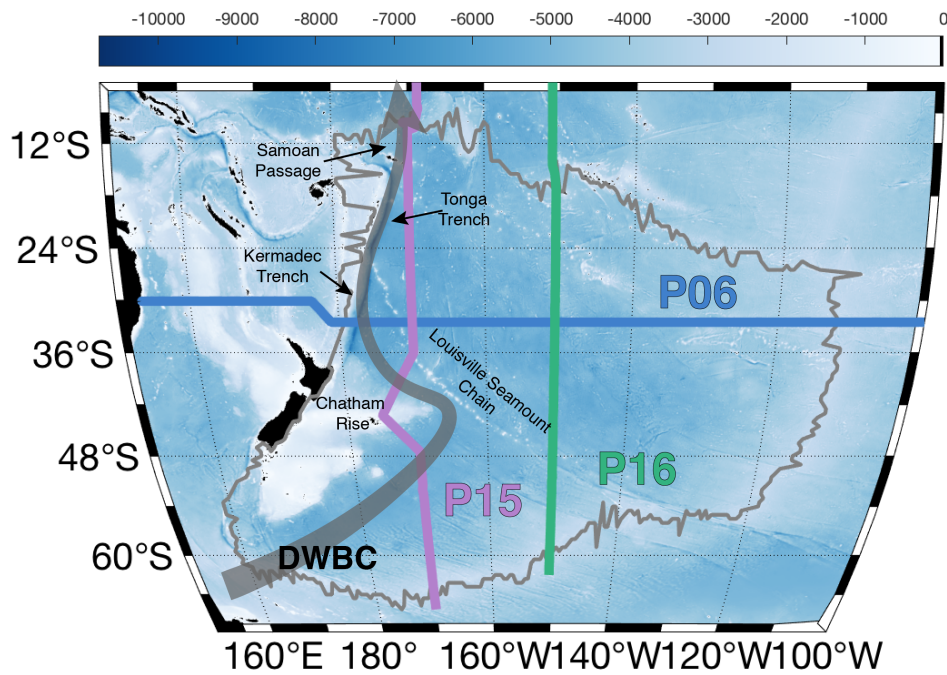
77 Stratification change affects the medium of local dynamics, which can have feed-  
78 back effects on global climate. For example, this change can affect the generation of in-  
79 ternal waves due to barotropic tidal flow over uneven topography (Bell, 1975; Baines,  
80 1982; Garrett & Kunze, 2007). Globally, the tides input about 1 TW into the internal  
81 wave field, a significant portion of the total mixing required to close the MOC (Egbert  
82 & Ray, 2000; St. Laurent & Simmons, 2006; Waterhouse et al., 2014). Once internal waves  
83 are generated, stratification also affect their propagation, breaking, and subsequent tur-  
84 bulent dissipation (Gregg, 1989). Finally, it directly impacts the temperature gradient,  
85 which sets the vertical heat flux. Through multiple ways, stratification is linked to the  
86 vertical transport of water and heat, a key aspect of climate projections (Melet, Hall-  
87 berg, et al., 2013; Melet et al., 2014).

88 While the processes discussed above are global, it is valuable to analyze their ex-  
89 act mechanisms on a sub-basin scale. This paper focuses on the Southwest Pacific Basin,  
90 a key pathway in the transport of AABW (Fig. 1) that connects deep waters in the South-  
91 ern Ocean to the Pacific (Whitworth et al., 1999; Sloyan & Rintoul, 2001). As there is  
92 no deep water formation in the North Pacific, the bottom branch of the Pacific MOC  
93 is sourced exclusively from southern high latitudes and carried north via the DWBC. In  
94 the southern subtropical latitudes, despite mixing by the Antarctic Circumpolar Cur-  
95 rent, more than 70% of the water in the abyssal ocean is AABW in origin (Johnson, 2008).  
96 AABW is carried into the basin south of the Campbell Plateau, flowing northwards through  
97 the Kermadec and Tonga Trench, and exiting into the Pacific Basin via the Samoan Pas-  
98 sage (Fig. 1). In the Samoan Passage, most of the northward flow is below 0.85 °C (Roemmich  
99 et al., 1996; Voet et al., 2016). Since AABW warms as it travels north, within the scope  
100 of this paper, we shall define AABW to be everything colder than 0.8 °C.

105 Here we quantify the stratification change in the Southwest Pacific Basin from the  
106 1990s through 2017 and analyze the spatial pattern. Basin wide averages of the change  
107 in both stratification and heat flux are estimated. Finally, we discuss the implications  
108 and potential feedbacks.

## 109 **2 Data and Methods**

110 In this study, we use deep ocean temperature, salinity, and pressure data from re-  
111 peated ship-based hydrographic surveys to determine the decadal rate of change of sec-



101 **Figure 1.** A map of the Southwest Pacific Basin bathymetry. The grey outline indicates the  
 102 basin boundary (Purkey & Johnson, 2010). WOCE sections considered in this analysis are depicted,  
 103 and key topographical features are labeled for reference. The grey arrow represents the  
 104 approximate pathway of the Deep Western Boundary Current (Whitworth et al., 1999).

112 ond order characteristics in the abyssal Southwest Pacific Basin. This data is first col-  
 113 lected in the 1990s by the World Ocean Circulation Experiment (WOCE), which con-  
 114 ducted full-depth high resolution CTD surveys along sections transecting the world’s oceans.  
 115 This effort is sustained through the 2000s and 2010s by the Climate Variability and Pre-  
 116 dictability (CLIVAR) program, and currently by the Global Ocean-Based Hydrographic  
 117 Investigations Program (GO-SHIP).

118 We consider a latitudinal section, P06, and two longitudinal sections P15 and P16  
 119 (Fig. 1). P06 (blue line) provides a zonal cross section of northward bottom water trans-  
 120 port while P15 and P16 (purple and green lines) capture a meridional view. P06 was oc-  
 121 cupied in 1992, 2003, 2010, and 2017, P15 in 1996, 2001, 2009, and 2016, and P16 in 1992,  
 122 2005, and 2014. CTD samples are nominally spaced 55 km apart. Temperature and salin-  
 123 ity observations are made from the surface to within 10-20 m of the seafloor and initially  
 124 binned into 1 or 2 dbar pressure grids. The instrumental accuracy for temperature, salin-  
 125 ity, and pressure profiles are  $\pm 0.002^\circ\text{C}$ ,  $\pm 0.002$  PSS-78, and  $\pm 3$  dbar respectively (Hood  
 126 et al., 2010). For more accurate salinity comparisons between occupations, batch-to-batch  
 127 salinity offsets are applied following Kawano et al. (2006).

128 The quality controlled temperature, salinity, and pressure data are used to calcu-  
 129 late absolute salinity ( $S_A$ ) and conservative temperature ( $\Theta$ ), the parameters of the TEOS-  
 130 10 toolbox used throughout the analysis (McDougall & Barker, 2011). Following the meth-  
 131 ods of Purkey and Johnson (2010), a 40-dbar half-width Hanning filter is applied to each  
 132  $S_A$  and  $\Theta$  profile, which is then interpolated onto a vertical 40 dbar pressure grid. This  
 133 coarser grid was chosen to minimize noise from transient eddies in the data in favor of  
 134 large scale changes. In each pressure bin, the data is then interpolated onto a  $2^\circ$  lati-  
 135 tude or longitude horizontal grid selected to encompass the most overlap between each  
 136 occupation. The maximum pressure of each profile is taken to be the seafloor depth, and  
 137 used to mask over any interpolated data.

138 We define stratification as the square of buoyancy frequency,  $N^2$ . This is calculated  
 139 for each grid point using,

$$140 \quad N^2 = g^2 \frac{\beta \Delta S_A - \alpha \Delta \Theta}{V_{sp} \Delta P} \quad (1)$$

141 where  $dS_A$  and  $d\Theta$  is the difference between the value at a given pressure bin with the  
 142 one above,  $\alpha$  and  $\beta$  are the thermal expansion and saline contraction coefficients respec-

143 tively,  $V_{sp}$  is the specific volume calculated using a 75-term polynomial expression, and  
 144  $P$  is pressure in Pascals (Roquet et al., 2015).

145 For each grid point, we also calculate vertical heat flux ( $Q$ ) using the equation,

$$146 \quad Q = \rho c_p \kappa N_\Theta^2 \quad (2)$$

147 where  $\rho$  and  $c_p$  are the density and heat capacity of seawater, both constants in this anal-  
 148 ysis.  $N_\Theta^2$  is the vertical gradient of conservative temperature, or  $\frac{\partial}{\partial z}\Theta$ . The diffusivity  $\kappa$ ,  
 149 is parameterized in two different ways. The first is the canonical constant value  $10^{-4}$  m<sup>2</sup>/s,  
 150 so that heat flux is proportional  $N_\Theta^2$  (Munk, 1966; Waterhouse et al., 2014). The sec-  
 151 ond is a gridded spatially variable diffusivity calculated using an average of the finescale  
 152 parameterization derived from  $N^2$  strain calculated for each occupation (K. L. Polzin  
 153 et al., 1995; Whalen et al., 2015). Since processing choices made in early occupations in-  
 154 fluence the data fine structure, we only use parameterized diffusivities from occupations  
 155 after 1995. Furthermore, as diffusivity is a log-normal variable, a geometric mean is used  
 156 to estimate the average value (Gurvich & Yaglom, 1967; Gregg, 1989).

## 157 **2.1 Isotherm Grid**

158 The gridded  $N^2$  and heat flux are reparameterized by density to eliminate effects  
 159 from isopycnal heave. Since salinity errors have a more significant impact on density, es-  
 160 pecially in the deep ocean, temperature is chosen as the independent variable (Purkey  
 161 & Johnson, 2013). Using  $\Theta$  from each occupation, the pressure binned values are piece-  
 162 wise cubic interpolated onto a 0.01°C grid. In this framework, each vertical bin repre-  
 163 sents a single temperature class. As we define AABW by temperature, this reparamete-  
 164 rization allows for comparisons between the water mass' properties over time, regard-  
 165 less of its vertical movement in the water column.

## 166 **2.2 Change over Time**

167 The change in  $N^2$  or heat flux over time is estimated using a linear fit across all  
 168 occupations of each section. Since the sections are re-occupied about once every decade,  
 169 changes are estimated on a decadal scale. To further minimize small scale fluctuations  
 170 with depth, we average the value of each bin with that of the bins above and below (ex-  
 171 cept along boundaries) prior to taking the fit.

172 Since  $N^2$  is a log-normal value (Gregg, 1989), we perform the linear fit on  $\log(N^2)$ .  
 173 By comparing the order of magnitude of  $N^2$ , rather than its absolute value,  $\frac{\partial}{\partial t}$  is an ex-  
 174 pression for the relative change over time. Thus,  $\frac{\partial}{\partial t} \log(N^2)$  is better expressed as a scal-  
 175 ing factor, defined as

$$s(N^2) = 10^{\frac{\partial}{\partial t} \log(N^2)} \quad (3)$$

176 For example,  $\frac{\partial}{\partial t} \log(N^2) = -0.1$  is equivalent to a factor of  $s = 0.8$ . Hence, every decade  
 177  $N^2$  is scaled by 0.8, or a 20% decrease. Using this method for all grid points, we pro-  
 178 duce a gridded map of  $s(N^2)$  for each section.

179 The data for P15 is different: only the first and last occupation sampled latitudes  
 180 south of 47.5°S. Change in this region is calculated separately based on the two occu-  
 181 pations.

### 182 **2.3 Basin Averages and Errors**

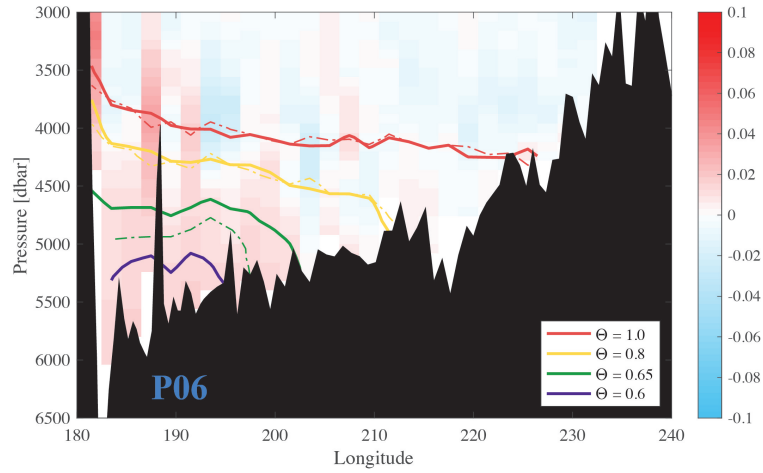
183 We estimate change in the total basin by calculating the length weighted mean and  
 184 standard deviation of all three sections. The study region is constrained within the bound-  
 185 aries of the Southwest Pacific Basin as defined by Purkey and Johnson (2010).

186 Confidence intervals are determined by calculating the degree of freedom (DOF)  
 187 of each temperature class, obtained by dividing the length of that isotherm by a hori-  
 188 zontal decorrelation length scale of 163 km (Purkey & Johnson, 2010). If the isotherm  
 189 is segmented by topography, each portion is assumed to be statistically independent and  
 190 contribute at least one DOF. The standard error is estimated by dividing the standard  
 191 deviation by the square root of the DOF. The 95% confidence interval is estimated us-  
 192 ing a Student's  $t$  distribution.

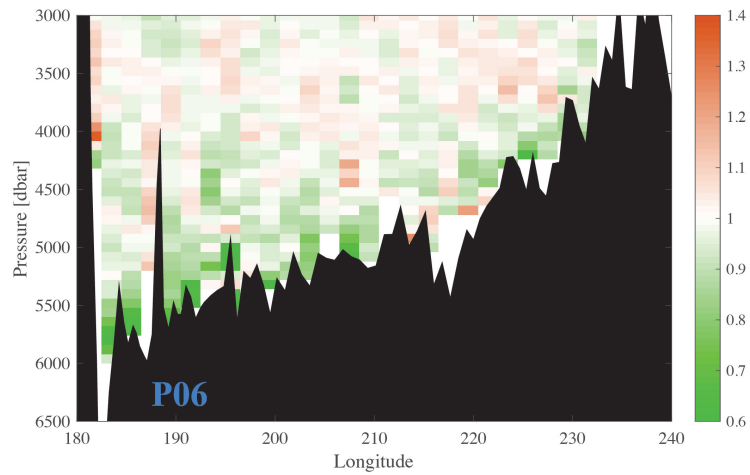
## 193 **3 Results**

194 Warming between 1990s-2010s is more prominent near the bottom, a trend which  
 195 has been observed in all three sections in this analysis and noted by multiple previous  
 196 studies (Purkey & Johnson, 2010; Sloyan et al., 2013; D. G. Desbruyères et al., 2016).  
 197 This warming is primarily observed below  $\Theta = 0.8$  °C, so that isotherms below this bound-  
 198 aries grow further apart. Since salinity effects are small, the increasing separation of isotherms  
 199 manifests as a reduction of stratification.

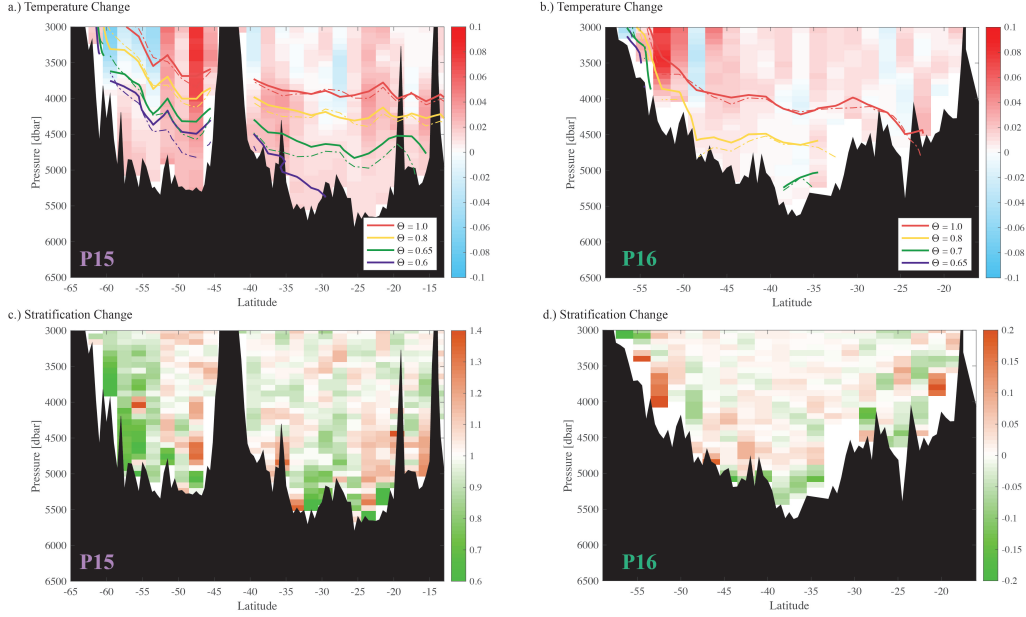
a.) Temperature Change



b.) Stratification Change



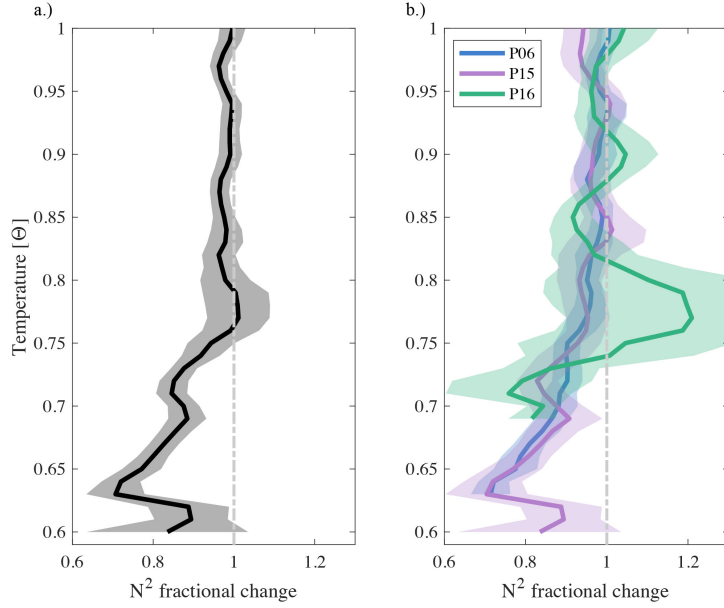
200 **Figure 2.** Decadal rate of change of conservative temperature  $d\Theta/dt$  along section P06 within  
 201 the basin. Warming regions are shaded in red while cooling regions are shaded blue. Contoured  
 202 isotherms from 1992 (solid line) and 2017 (dashed line) are depicted. (b) Decadal fractional  
 203 change of the Brunt Väisälä frequency  $N^2$ . Decreasing  $N^2$  is shaded green, increasing  $N^2$  shaded  
 204 orange. The seafloor is masked over in black.



222 **Figure 3.** Decadal conservative temperature rate of change (a-b) and  $N^2$  fractional change  
 223 (c-d) along sections P15 and P16 following Fig. 2

205 The average decadal warming below  $\Theta = 1.0$  °C section P06 is of  $\mathcal{O}(10^{-3})$  °C (Fig.  
 206 2 a). This is an order of magnitude greater than the average observed warming above  
 207  $\Theta = 0.8$  °C and below  $\Theta = 1.0$  °C. Abyssal warming is most prominent in the west-  
 208 ern side of the basin along the path of the DWBC (Fig. 2a). Within the AABW, warm-  
 209 ing is strongest near the sea floor. As a result, colder isotherms deeper in the water col-  
 210 umn have fallen at a faster rate. Between 1992 and 2017, the  $\Theta = 0.65$  °C isotherm  
 211 has fallen by 562.25 m, while the  $\Theta = 0.8$  °C isotherm only fell by 14.17 m. Further  
 212 down the water column, the  $\Theta = 0.6$  °C isotherm has completely disappeared by 2017,  
 213 indicating an absence of the coldest waters. In contrast, warmer isotherms such as  $\Theta =$   
 214  $1.0$  °C have remained relatively stationary due to minimal temperature changes.

215 Another consequence of changing bottom water properties is a reduction of near  
 216 bottom stratification (Fig. 2b). The stratification change over time  $\frac{\partial}{\partial t} N^2$  is concentrated  
 217 along the seafloor. The biggest decrease is observed in the Kermadec Trench around  $183^\circ$ ,  
 218 where  $N^2$  has dropped by approximately 40% per decade. Both  $\frac{\partial}{\partial t} \Theta$  and  $\frac{\partial}{\partial t} N^2$  show a  
 219 stronger warming/reduction on the western side of the basin, which is spatially consist-  
 220 ent with the path of AABW as it flows northward with the DWBC (Fig. 1). On the  
 221 eastern side, a smaller  $N^2$  reduction is observed along the East Pacific Rise.

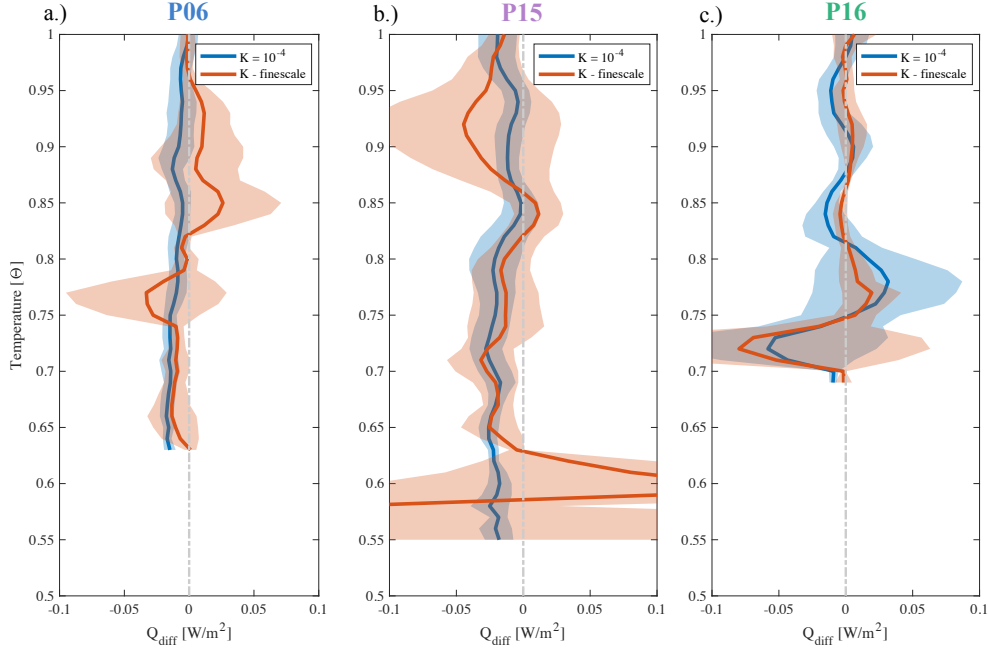


235 **Figure 4.** Average decadal  $N^2$  fraction change in conservative temperature coordinates (a)  
 236 weighted by length for all basin sections (b) for each section.

224 The two meridional sections, P15 in the west and P16 in the east also show increased  
 225 warming below  $\Theta = 0.8$  °C (Fig. 3a,b). Isotherms slant towards the seafloor in the east-  
 226 ern half the the basin. Thus, there is a higher fraction of AABW in the western half of  
 227 the basin leading to lower temperatures and increased warming: below 4000 dbar P15  
 228 is 0.1 °C colder on average than P16, and warming 90% more per decade.

229 The  $N^2$  changes along the longitudinal sections (Fig. 3c,d) exhibit more horizon-  
 230 tal variability, which can also be observed in  $\frac{\partial}{\partial t}\Theta$ . Both sections P15 and P16 show a  
 231 near bottom reduction in  $N^2$ , particularly below 5000 dbar. In P15, the strongest  $N^2$   
 232 decrease is observed south of 55°S where AABW is advected into the basin, and in the  
 233 deepest region between 20°S and 35°S (Fig. 3 c). In P16, we observe the most substan-  
 234 tial  $N^2$  reduction between 45°S and 35°S.

237 Averaged across all sections, we find a statistically significant  $N^2$  decrease below  
 238  $\Theta = 0.75$  °C. Despite variability across isobaths, decadal  $\frac{\partial}{\partial t}N^2$  is fairly consistent along  
 239 isotherm surfaces (Fig. 4). The stratification reduction rate is greater in colder temper-  
 240 ature classes at depth. At the AABW boundary ( $\Theta = 0.8$  °C) the average factor change  
 241 is around 0.95, or a 5% percent reduction per decade. In comparison, the  $\Theta = 0.63$  °C  
 242 temperature class has a factor change of  $0.71 \pm 0.07$ , which corresponds to a  $N^2$  reduc-



252 **Figure 5.** Decadal heat flux change ( $\frac{\partial Q}{\partial t}$ ) for (a) P06 (b) P15 and (c) P16. The blue line  
 253 represents heat flux calculated using a constant diffusivity of  $10^{-4} \text{ m}^2 \text{ s}^{-1}$  and the orange line  
 254 represents heat flux calculated using a spatially variable  $\kappa$  based on finescale strain parameteriza-  
 255 tion.

243 tion of almost 30%.  $N^2$  decrease is observed primarily in the averaged profiles of P06  
 244 and P15 (Fig.4b). These two sections contain a significant fraction of AABW, and  $N^2$   
 245 is significantly decreasing with good agreement in AABW temperatures down to  $\Theta =$   
 246  $0.63 \text{ }^\circ\text{C}$ . Below this isotherm, all data comes from a small region at the southern end of  
 247 P15, leading to greater uncertainty. In contrast, P16 does not show significant  $N^2$  de-  
 248 crease except in DWBC pathway along the base of the East Pacific Rise and therefore  
 249 samples a smaller fraction of AABW. At and below  $\Theta = 0.8 \text{ }^\circ\text{C}$ , there is significant spa-  
 250 tial variability and the change is not statistically distinguishable from zero until below  
 251  $\Theta = 0.73$ , where the  $N^2$  reduction is comparable with that of P06 and P15.

256 Similarly, heat flux is also decreasing as a function of time, as approximated from  
 257  $N_\Theta^2$  (Fig.5). Unlike  $N^2$ , the trend is calculated linearly, and the change is an absolute  
 258 value. With a constant diffusivity of  $\kappa = 10^{-4} \text{ m}^2 \text{ s}^{-1}$ , the estimated heat flux trend  
 259 is  $\frac{\partial}{\partial t} N_\Theta^2$  scaled by a constant. Using this simplified method, we find an average per decade  
 260 heat flux reduction of  $0.016 \pm 0.01 \text{ W m}^{-2}$  below  $\Theta = 0.8 \text{ }^\circ\text{C}$ . The sections containing

261 more AABW, P06 and P15, show similar patterns of heat flux reduction, likely associ-  
 262 ated with the warming of the AABW. Further away from its pathway, there is no sig-  
 263 nificant heat flux reduction in P16 except below  $\Theta = 0.70$  °C.

264 Using a spatially (but not temporally) variable diffusivity estimate (Whalen et al.,  
 265 2015), the average heat flux reduction below  $\Theta = 0.8$  °C is  $0.041 \pm 0.1$  Wm<sup>-2</sup>. The  
 266 confidence interval is much wider and the change is not statistically significant. This is  
 267 due in part to the wide range of diffusivities from  $10^{-5}$  m<sup>2</sup>s<sup>-1</sup> in the basin interior up  
 268 to  $10^{-3}$  m<sup>2</sup>s<sup>-1</sup> right above the seafloor (K. Polzin et al., 1997). Despite large confidence  
 269 intervals in general, there is a significant reduction in a few temperature classes of P06  
 270 and in P15 between  $\Theta = 0.73$  °C and  $\Theta = 0.68$  °C

## 271 4 Summary and Discussion

272 A significant  $N^2$  decrease is observed in the Southwest Pacific Basin for water be-  
 273 low  $\Theta = 0.8$  °C based on hydrography observations between the 1990s and 2010s. Our  
 274 analysis agrees with previous results that show a significant warming of AABW along  
 275 the DWBC in the Southwest Pacific Basin (Sloyan et al., 2013). In addition, we present  
 276 observations that show that stronger warming at depth leads to a significant reduction  
 277 of stratification at depth in all three chosen study sections of the Southwest Pacific Basin:  
 278 P06, P15, and P16.

279 A consequence of changing stratification is that it alters the medium of internal wave  
 280 generation, propagation, and dissipation, the main driver of mixing in the deep ocean  
 281 (St. Laurent & Garrett, 2002; Waterhouse et al., 2014). The energy conversion from barotropic  
 282 tidal flow over uneven topography to internal gravity waves scales with  $N$  (Bell, 1975;  
 283 Garrett & Kunze, 2007; Melet, Nikurashin, et al., 2013). Once generated, the average  
 284 energy dissipation rate of internal waves  $\langle \epsilon \rangle$  is proportional to  $N^2$  (Gregg, 1989; K. L. Polzin  
 285 et al., 2014). In the upper ocean, increased surface heating has created a stronger strat-  
 286 ification, which is linked to more internal wave activity and turbulent energy dissipation  
 287 (Capotondi et al., 2012; DeCarlo et al., 2015). In contrast, we find a significant  $N^2$  re-  
 288 duction in near bottom isotherms that is enhanced with depth. Consequently, we expect  
 289 a decrease in both internal wave tidal energy conversion and turbulent dissipation rate  
 290 by the respective scaling relations of Bell (1975) and Gregg (1989). Preliminary anal-  
 291 ysis of tidal energy change shows a statistically insignificant decrease of  $(3.64 \pm 8.18) \times$

292  $10^{-4} \text{ Wm}^{-2}$  averaged across all three sections in the basin. The wide error interval is  
293 a product of low signal to noise ratio and the sensitivity of tidal energy conversion to the  
294 topographical variations within the basin (Melet, Nikurashin, et al., 2013). However, re-  
295 cent studies have shown that warming in the Southwest Pacific has accelerated in the  
296 2010s compared to previous decades (Johnson et al., 2019; Purkey et al., 2019). Since  
297 we find that  $N^2$  decrease correlates to bottom intensified warming, the accelerated warm-  
298 ing may lead to an accelerated  $N^2$  reduction. If this trend continues, the impact on in-  
299 ternal waves could become more significant in the coming decades.

300 In addition to stratification decrease, a weakening temperature gradient results in  
301 a smaller downward heat flux. The magnitude of the estimated trend is dependent on  
302 whether the diffusivity  $\kappa$  is assumed to be spatially uniform or varying. With uniform  
303 diffusivity, the estimated heat flux change is proportional to the changing temperature  
304 gradient. Considering the spatial variation of diffusivity accounts for enhanced mixing  
305 over rough topography (Ledwell et al., 2000). Since abyssal temperature profiles are rel-  
306 atively homogeneous, a single temperature class may reside in both strong and weak mix-  
307 ing environments, increasing the variance of heat flux change along each  $\Theta$  value, widen-  
308 ing the confidence interval. Heat flux change estimates using both a constant and spa-  
309 tially variable parameterizations of diffusivity show a decreasing trend in downward heat  
310 flux over the past three decades. As a result, less heat (and thus buoyancy) is mixed into  
311 the deep ocean from above. Over time, this can allow the water column to re-stratify,  
312 potentially reversing the observed trend. Additionally, the observed decrease of abyssal  
313 heat flux could reduce the ability of the deep ocean to act as a heat sink for the warm-  
314 ing upper ocean, although this may be corrected by the negative feedback loop. More  
315 research is needed to examine the timescales of these changes and feedbacks, which should  
316 be considered both locally and on a global scale.

317 This study suggests a connection between stratification and heat flux change, which  
318 is potentially linked to future changes in internal wave generation and dissipation. Both  
319  $N^2$  and turbulent dissipation are important for upwelling, and an alteration of these terms  
320 will have consequences for the strength of the abyssal MOC (Furue & Endoh, 2005; Jayne,  
321 2009; Oka & Niwa, 2013; Hieronymus et al., 2019). However, current efforts have yet to  
322 untangle the relative interconnected contributions. While bottom warming is almost ubiq-  
323 uitous in the world's oceans, much is still unknown about stratification change in other  
324 basins and how it relates to global mixing processes, heat flux, and ocean circulation.

325 Since vertical transport of heat and water is key for accurate climate projections (Melet,  
326 Hallberg, et al., 2013), more deep ocean research and data, such as the establishment  
327 of a Deep Argo program (Johnson et al., 2015), is critical to improving predictions of fu-  
328 ture climate change.

### 329 **Acknowledgments**

330 CBW and HJZ were supported by the National Science Foundation Award OCE-1923558  
331 and the University of Washington Royalty Research Fund. SGP was supported by US  
332 GO-SHIP (NSF OCE-1437015) and the CLIVAR and Carbon Hydrographic Data Of-  
333 fice (NSF OCE 1829814 and NOAA NA15OAR4320071). GO-SHIP CTD hydrography  
334 data is publicly available from CCHDO (<https://cchdo.ucsd.edu/>). We are grateful  
335 for the PIs, cruise participants, and ship officers and crew who helped collect, calibrate,  
336 and process this data.

### 337 **References**

- 338 Baines, P. G. (1982). On internal tide generation models. *Deep Sea Research Part*  
339 *A. Oceanographic Research Papers*, 29(3), 307–338.
- 340 Bell, T. (1975). Topographically generated internal waves in the open ocean. *J. Geo-*  
341 *phys. Res.*, 80(3), 320–327.
- 342 Capotondi, A., Alexander, M. A., Bond, N. A., Curchitser, E. N., & Scott, J. D.  
343 (2012). Enhanced upper ocean stratification with climate change in the CMIP3  
344 models. *Journal of Geophysical Research: Oceans*, 117(C4).
- 345 Castagno, P., Capozzi, V., DiTullio, G. R., Falco, P., Fusco, G., Rintoul, S. R., ...  
346 Budillon, G. (2019). Rebound of shelf water salinity in the Ross sea. *Nature*  
347 *communications*, 10(1), 1–6.
- 348 DeCarlo, T. M., Karnauskas, K. B., Davis, K. A., & Wong, G. T. (2015). Climate  
349 modulates internal wave activity in the Northern South China Sea. *Geophys-*  
350 *ical Research Letters*, 42(3), 831–838.
- 351 De Lavergne, C., Madec, G., Le Sommer, J., Nurser, A. G., & Naveira Garabato,  
352 A. C. (2016). On the consumption of antarctic bottom water in the abyssal  
353 ocean. *Journal of Physical Oceanography*, 46(2), 635–661.
- 354 Desbruyères, D., McDonagh, E. L., King, B. A., & Thierry, V. (2017). Global and  
355 full-depth ocean temperature trends during the early twenty-first century from

- 356 argo and repeat hydrography. *Journal of Climate*, *30*(6), 1985–1997.
- 357 Desbruyères, D. G., Purkey, S. G., McDonagh, E. L., Johnson, G. C., & King, B. A.  
358 (2016). Deep and abyssal ocean warming from 35 years of repeat hydrography.  
359 *Geophysical Research Letters*, *43*(19), 10–356.
- 360 Egbert, G., & Ray, R. (2000). Significant dissipation of tidal energy in the deep  
361 ocean inferred from satellite altimeter data. *Nature*, *405*(6788), 775–778.
- 362 England, M. H. (1995). The age of water and ventilation timescales in a global  
363 ocean model. *Journal of Physical Oceanography*, *25*(11), 2756–2777.
- 364 Furue, R., & Endoh, M. (2005). Effects of the Pacific diapycnal mixing and wind  
365 stress on the global and Pacific meridional overturning circulation. *Journal of*  
366 *physical oceanography*, *35*(10), 1876–1890.
- 367 Garrett, C., & Kunze, E. (2007). Internal tide generation in the deep ocean. *Annu.*  
368 *Rev. Fluid Mech.*, *39*, 57–87.
- 369 Gregg, M. (1989). Scaling turbulent dissipation in the thermocline. *Journal of Geo-*  
370 *physical Research: Oceans*, *94*(C7), 9686–9698.
- 371 Gurvich, A., & Yaglom, A. (1967). Breakdown of eddies and probability distribu-  
372 tions for small-scale turbulence. *The Physics of Fluids*, *10*(9), S59–S65.
- 373 Hieronymus, M., Nycander, J., Nilsson, J., Döös, K., & Hallberg, R. (2019). Oceanic  
374 overturning and heat transport: The role of background diffusivity. *Journal of*  
375 *Climate*, *32*(3), 701–716.
- 376 Hood, E., Sabine, C., & Sloyan, B. (2010). GO-SHIP Repeat Hydrography Manual,  
377 Version 1: Cover page and contents.
- 378 Jacobs, S. S., & Giulivi, C. F. (2010). Large multidecadal salinity trends near the  
379 Pacific–Antarctic continental margin. *Journal of Climate*, *23*(17), 4508–4524.
- 380 Jayne, S. R. (2009). The impact of abyssal mixing parameterizations in an ocean  
381 general circulation model. *Journal of Physical Oceanography*, *39*(7), 1756–  
382 1775.
- 383 Johnson, G. C. (2008). Quantifying Antarctic bottom water and North Atlantic  
384 deep water volumes. *Journal of Geophysical Research: Oceans*, *113*(C5).
- 385 Johnson, G. C., Lyman, J. M., & Purkey, S. G. (2015). Informing deep argo array  
386 design using argo and full-depth hydrographic section data. *Journal of Atmo-*  
387 *spheric and Oceanic Technology*, *32*(11), 2187–2198.
- 388 Johnson, G. C., Mecking, S., & Sloyan, S. E., BernadeWijffels. (2007). Recent bot-

- 389 tom water warming in the Pacific Ocean. *Journal of Climate*, 20(21), 5365–  
390 5375.
- 391 Johnson, G. C., Purkey, S. G., & Toole, J. M. (2008). Reduced antarctic meridional  
392 overturning circulation reaches the north atlantic ocean. *Geophysical Research*  
393 *Letters*, 35(22).
- 394 Johnson, G. C., Purkey, S. G., Zilberman, N. V., & Roemmich, D. (2019). Deep  
395 Argo quantifies bottom water warming rates in the southwest Pacific Basin.  
396 *Geophysical Research Letters*, 46(5), 2662–2669.
- 397 Kawano, T., Aoyama, M., Joyce, T., Uchida, H., Takatsuki, Y., & Fukasawa, M.  
398 (2006). The latest batch-to-batch difference table of standard seawater and its  
399 application to the WOCE onetime sections. *Journal of oceanography*, 62(6),  
400 777–792.
- 401 Kouketsu, S., Doi, T., Kawano, T., Masuda, S., Sugiura, N., Sasaki, Y., ... oth-  
402 ers (2011). Deep ocean heat content changes estimated from observation  
403 and reanalysis product and their influence on sea level change. *Journal of*  
404 *Geophysical Research: Oceans*, 116(C3).
- 405 Kouketsu, S., Fukasawa, M., Kaneko, I., Kawano, T., Uchida, H., Doi, T., ... Mu-  
406 rakami, K. (2009). Changes in water properties and transports along 24 n in  
407 the north pacific between 1985 and 2005. *Journal of Geophysical Research:*  
408 *Oceans*, 114(C1).
- 409 Ledwell, J., Montgomery, E., Polzin, K., Laurent, L. S., Schmitt, R., & Toole, J.  
410 (2000). Evidence for enhanced mixing over rough topography in the abyssal  
411 ocean. *Nature*, 403(6766), 179–182.
- 412 Lumpkin, R., & Speer, K. (2007). Global ocean meridional overturning. *Journal of*  
413 *Physical Oceanography*, 37(10), 2550–2562.
- 414 Masuda, S., Awaji, T., Sugiura, N., Matthews, J. P., Toyoda, T., Kawai, Y., ... oth-  
415 ers (2010). Simulated rapid warming of abyssal North Pacific waters. *Science*,  
416 329(5989), 319–322.
- 417 McDougall, T. J., & Barker, P. M. (2011). Getting started with TEOS-10 and the  
418 Gibbs Seawater (GSW) oceanographic toolbox. *SCOR/IAPSO WG*, 127, 1–  
419 28.
- 420 Melet, A., Hallberg, R., Legg, S., & Nikurashin, M. (2014). Sensitivity of the ocean  
421 state to lee wave-driven mixing. *Journal of physical oceanography*, 44(3), 900–

- 422 921.
- 423 Melet, A., Hallberg, R., Legg, S., & Polzin, K. (2013). Sensitivity of the ocean state  
424 to the vertical distribution of internal-tide-driven mixing. *Journal of Physical*  
425 *Oceanography*, *43*(3), 602–615.
- 426 Melet, A., Nikurashin, M., Muller, C., Falahat, S., Nycander, J., Timko, P. G., ...  
427 Goff, J. A. (2013). Internal tide generation by abyssal hills using analytical  
428 theory. *Journal of Geophysical Research: Oceans*, *118*(11), 6303–6318.
- 429 Munk, W. H. (1966). Abyssal recipes. In *Deep sea research and oceanographic ab-*  
430 *stracts* (Vol. 13, pp. 707–730).
- 431 Nikurashin, M., & Ferrari, R. (2013). Overtuning circulation driven by breaking  
432 internal waves in the deep ocean. *Geophysical Research Letters*, *40*(12), 3133–  
433 3137.
- 434 Oka, A., & Niwa, Y. (2013). Pacific deep circulation and ventilation controlled by  
435 tidal mixing away from the sea bottom. *Nature communications*, *4*(1), 1–8.
- 436 Orsi, A. H., Johnson, G. C., & Bullister, J. L. (1999). Circulation, mixing, and pro-  
437 duction of Antarctic Bottom Water. *Progress in Oceanography*, *43*(1), 55–109.
- 438 Polzin, K., Toole, J., Ledwell, J., & Schmitt, R. (1997). Spatial variability of turbu-  
439 lent mixing in the abyssal ocean. *Science*, *276*(5309), 93–96.
- 440 Polzin, K. L., Garabato, A. C. N., Huussen, T. N., Sloyan, B. M., & Waterman,  
441 S. (2014). Finescale parameterizations of turbulent dissipation. *Journal of*  
442 *Geophysical Research: Oceans*, *119*(2), 1383–1419.
- 443 Polzin, K. L., Toole, J. M., & Schmitt, R. W. (1995). Finescale parameterizations of  
444 turbulent dissipation. *Journal of physical oceanography*, *25*(3), 306–328.
- 445 Purkey, S. G., & Johnson, G. C. (2010). Warming of global abyssal and deep South-  
446 ern Ocean waters between the 1990s and 2000s: Contributions to global heat  
447 and sea level rise budgets. *Journal of Climate*, *23*(23), 6336–6351.
- 448 Purkey, S. G., & Johnson, G. C. (2012). Global contraction of Antarctic Bottom  
449 Water between the 1980s and 2000s. *Journal of Climate*, *25*(17), 5830–5844.
- 450 Purkey, S. G., & Johnson, G. C. (2013). Antarctic Bottom Water warming and  
451 freshening: Contributions to sea level rise, ocean freshwater budgets, and  
452 global heat gain. *Journal of Climate*, *26*(16), 6105–6122.
- 453 Purkey, S. G., Johnson, G. C., Talley, L. D., Sloyan, B. M., Wijffels, S. E., Smethie,  
454 W., ... Katsumata, K. (2019). Unabated Bottom Water Warming and Fresh-

- 455 ening in the South Pacific Ocean. *Journal of Geophysical Research: Oceans*,  
456 *124*(3), 1778–1794. doi: 10.1029/2018JC014775
- 457 Rignot, E., Mouginot, J., Scheuchl, B., van den Broeke, M., van Wessem, M. J.,  
458 & Morlighem, M. (2019). Four decades of antarctic ice sheet mass balance  
459 from 1979–2017. *Proceedings of the National Academy of Sciences*, *116*(4),  
460 1095–1103.
- 461 Roemmich, D., Hautala, S., & Rudnick, D. (1996). Northward abyssal transport  
462 through the Samoan Passage and adjacent regions. *Journal of Geophysical Re-*  
463 *search: Oceans*, *101*(C6), 14039–14055.
- 464 Roquet, F., Madec, G., McDougall, T. J., & Barker, P. M. (2015). Accurate poly-  
465 nomial expressions for the density and specific volume of seawater using the  
466 teos-10 standard. *Ocean Modelling*, *90*, 29–43.
- 467 Sloyan, B. M., & Rintoul, S. R. (2001). The southern ocean limb of the global deep  
468 overturning circulation. *Journal of Physical Oceanography*, *31*(1), 143–173.
- 469 Sloyan, B. M., Wijffels, S. E., Tilbrook, B., Katsumata, K., Murata, A., & Mac-  
470 donald, A. M. (2013). Deep ocean changes near the western boundary of the  
471 South Pacific Ocean. *Journal of physical oceanography*, *43*(10), 2132–2141.
- 472 St. Laurent, L., & Garrett, C. (2002). The role of internal tides in mixing the deep  
473 ocean. *Journal of Physical Oceanography*, *32*(10), 2882–2899.
- 474 St. Laurent, L., & Simmons, H. (2006). Estimates of power consumed by mixing in  
475 the ocean interior. *Journal of climate*, *19*(19), 4877–4890.
- 476 Talley, L. D. (2013). Closure of the global overturning circulation through the In-  
477 dian, Pacific, and Southern Oceans: Schematics and transports. *Oceanography*,  
478 *26*(1), 80–97.
- 479 Talley, L. D., Reid, J. L., & Robbins, P. E. (2003). Data-based meridional over-  
480 turning streamfunctions for the global ocean. *Journal of Climate*, *16*(19),  
481 3213–3226.
- 482 Voet, G., Alford, M. H., Girton, J. B., Carter, G. S., Mickett, J. B., & Klymak,  
483 J. M. (2016). Warming and weakening of the abyssal flow through Samoan  
484 Passage. *Journal of Physical Oceanography*, *46*(8), 2389–2401.
- 485 Waterhouse, A. F., MacKinnon, J. A., Nash, J. D., Alford, M. H., Kunze, E., Sim-  
486 mons, H. L., . . . Lee, C. M. (2014). Global patterns of diapycnal mixing from  
487 measurements of the turbulent dissipation rate. *J. Phys. Oceanogr.*, 1854–1872.

488 doi: 10.1175/JPO-D-13-0104.1

489 Whalen, C. B., MacKinnon, J. A., Talley, L. D., & Waterhouse, A. F. (2015). Es-  
490 timating the mean diapycnal mixing using a finescale strain parameterization.

491 *Journal of Physical Oceanography*, 45(4), 1174–1188.

492 Whitworth, T., Warren, B., Nowlin Jr, W., Rutz, S., Pillsbury, R., & Moore, M.

493 (1999). On the deep western-boundary current in the Southwest Pacific Basin.

494 *Progress in Oceanography*, 43(1), 1–54.